



OPEN

Large photocurrent density enhancement assisted by non-absorbing spherical dielectric nanoparticles in a GaAs layer

Bhaskar Singh^{1✉}, Mohammed M. Shabat² & Daniel M. Schaadt¹

Herein, we report a theoretical investigation of large photocurrent density enhancement in a GaAs absorber layer due to non-absorbing spherical dielectric (SiO₂) nanoparticles-based antireflection coating. The nanoparticles are embedded in a dielectric matrix (SiN) which improves the antireflection property of SiN ($\lambda/4$ coating) and let to pass more photons into the GaAs layer. The improvement is noticed omnidirectional and the highest is more than 100% at 85° angle of incidence with the nanoparticles' surface filling density of 70%. Sunrise to sunset calculation of normalized photocurrent density over the course of a year have also shown improvements in the nanoparticles' case.

Nanoparticles (NPs) are being used extensively in solar cell applications due to its high forward to backward scattering^{1–6}. This is caused by suppression of light reflection via high refractive index substrate (famously known as Kerker effect)⁷. Nanostructures such as NPs with size greater than and/or of the order of incident sunlight wavelength show Mie scattering. Additionally, metal NPs also show plasmonic scattering due to the oscillation of free electrons at metal-dielectric interface^{1,8}. However, metal NPs face high absorption at the resonance wavelength. On the other hand, dielectric NPs do not show this behavior in a narrow band range⁹. This have captured the attention of scientific community recently and being investigated widely. Dielectric NPs at the front of solar cells have been demonstrated experimentally^{10–15} and theoretically^{8,16–19} with improved device performance. Wan et al.'s TiO₂ NPs coated solar cell exhibited ca. 30% enhancement in photocurrent¹³. Whereas, Ha et al. demonstrated experimentally more than 30% efficiency gain by using SiO₂ NPs on a GaAs solar cell¹⁴. These NPs were closely packed and worked as an antireflection coating (ARC). The wide-angle improvement was also noticed for the entire visible spectrum. Huang et al. measured the normalized current density of with/without sub micrometer silica (SiO₂) spheres coated amorphous silicon (a-Si) solar cells and noticed the enhancement after 40° angle of incidence (AOI)²⁰.

In this manuscript, we perform an analytical modelling on a structure in which SiO₂ NPs are embedded in a dielectric ARC (SiN), also called $\lambda/4$ coating, on a GaAs layer. The new ARC structure with NPs is called hybrid ARC. We use a dipole model to describe the diffuse reflectance/transmittance behavior of NPs²¹. However, the specular behavior of SiN ARC layer is characterized by Abelès' famous transfer matrix method (TMM)²². The analytical model is presented in detail elsewhere²³. The hybrid ARC made of two-dimensional (2D) array of the SiO₂ NPs of equal period in the dielectric SiN matrix bounded with air and a GaAs absorber layer was investigated, as shown in Fig. 1. All the layers and NPs have wavelength dependent index of refraction which is taken from Palik for the calculation²⁴. AOI varies from normal incidence (0°) to 85°. NPs' surface filling density (f) is calculated by $f = N * (\pi r^2) / (l * b)$, where N is the total no. of embedded NPs; r is the radius of NPs; l is length, and b is breadth of SiN layer. The dipole approximation is valid for $f < 0.75$.

The ARCs in solar cells are designed to minimize the reflectance and maximize the transmittance across the wavelength range of interest. Figure 2 shows the weighted solar power transmittance: $T_w = \int_{300nm}^{1200nm} T(\lambda)S(\lambda)d\lambda / \int_{300nm}^{1200nm} S(\lambda)d\lambda$, where $T(\lambda)$ and $S(\lambda)$ are the transmittance from the ARC layer and the intensity of AM1.5D solar spectrum at wavelength λ . The intensity of AM1.5D solar spectrum is taken from

¹Institute of Energy Research and Physical Technologies, Clausthal University of Technology, Leibnizstraße 4, 38678 Clausthal-Zellerfeld, Germany. ²Physics Department, Islamic University of Gaza, P. O. Box 108, Gaza Strip, The Palestinian Authority. ✉email: bhaskar.singh@tu-clausthal.de

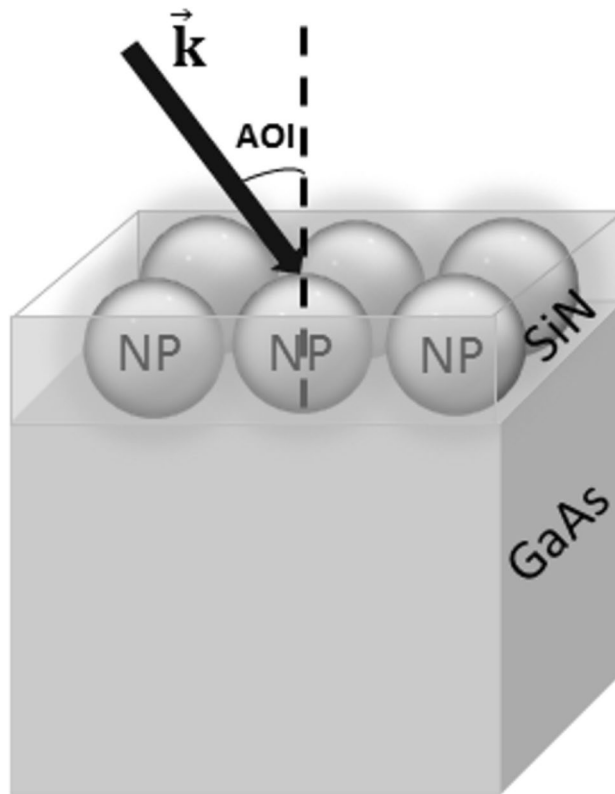


Figure 1. Schematic diagram of the simulated structure.

Ref.²⁵. Thin film SiN ARC layer shows high transmittance for the thickness 60–80 nm over a wide range of AOI (Fig. 2A). When the ARC layer thickness increases, the transmittance decreases slowly at normal incidence, however with AOI, the change is drastic after 40° AOI. A fixed solar cell on a house roof, receives the sun light throughout a day at various AOI. Thus, the ARC should perform better at higher AOI. Embedding Ag NPs in the SiN ARC shows better performance at higher AOI (Fig. 2B). However, the performance is bad at normal incidence comparing to the thin film SiN ARC because metal NPs absorb the sunlight, and SiN layer doesn't absorb⁹. Figure 2B also shows an expected behavior that metal NPs have large optical cross section than geometrical cross section²⁶. Smaller Ag NPs (blue region in Fig. 2B) absorb almost all the sunlight incident upon it. Therefore, we replaced metal NPs (Ag NPs) with dielectric NPs (SiO₂ NPs) because dielectric NPs do not absorb the sunlight in a narrow band spectrum as discussed in the beginning. The weighted solar power transmittance from hybrid ARC (SiO₂ NPs + SiN) is shown in Fig. 2C. SiN ARC and hybrid ARC (SiO₂ NPs + SiN) show nearly the same behavior for ARC thickness interval 60–80 nm at AOI 0°–40°. Furthermore, the improvement in transmittance from hybrid ARC (SiO₂ NPs + SiN) is omnidirectional. For comparison, we also calculated the transmittance for 100% SiO₂ thin film layer as ARC which shows a decrease in the transmittance at higher AOI (Fig. 2D). From the principle of single layer antireflection coating¹³, the refractive index of a perfect ARC should follow the following expression: $n_{ARC} = \sqrt{n_{Air} * n_{Substrate}}$. If we take $n_{Substrate} = 3.5$ (for GaAs or Si), n_{ARC} equals to 1.87. The refractive index of SiN (n_{SiN}) and SiO₂ (n_{SiO_2}) is 2.05 and 1.5 approx., respectively. Hence, n_{SiN} is near to n_{ARC} , but n_{SiO_2} is far from that. According to the effective medium theory¹³, embedding SiO₂ NPs in the SiN dielectric matrix brings the effective refractive index nearer to n_{ARC} , therefore we obtained the best ARC performance in the hybrid ARC (SiO₂ NPs + SiN).

In the solar cell application, photocurrent density (J_{PH}) is more commonly discussed property of a solar cell than the transmittance. So, we calculated $J_{PH} = q * \int_{300nm}^{870nm} T(\lambda) PFD(\lambda) IQE(\lambda) d\lambda$, where q is the electronic charge; $PFD(\lambda)$ and $IQE(\lambda)$ are the photon flux density and the internal quantum efficiency at wavelength λ . The photon flux density is taken from Ref. ²⁷. Operating wavelength is taken from 300 to 870 nm because GaAs absorbs the sunlight in this wavelength range. We assumed that all the photons which reaches to the GaAs layer, got absorbed; hence $IQE(\lambda) = 1, for all \lambda$. We plotted the weighted solar power transmittance (T_W) for an optimum condition of the hybrid ARC (SiO₂ NPs + SiN) at the surface filling density $f = 0.70$ and $d = 70nm$ (Fig. 3A). J_{PH} curves follow the same trend as T_W curves. J_{PH} is almost equal for the SiN ARC structure and the hybrid ARC (SiO₂ NPs + SiN) structure till 45° AOI, and after that the curves split (Fig. 3B). At 85° AOI, the improvement is as much as ca. 120% for the hybrid ARC (SiO₂ NPs + SiN) structure comparing to the SiN ARC. We also plotted J_{SC} and T_W curves of the hybrid ARC (SiO₂ NPs + SiN) at $f = 0.50$ (red curve in Fig. 3B), which is in between of the SiN ARC and the hybrid ARC (SiO₂ NPs + SiN) at $f = 0.70$. This means when f goes to zero, the hybrid ARC acts like the SiN ARC (as expected). With the help of Fig. 3B, we also calculated a net normalized

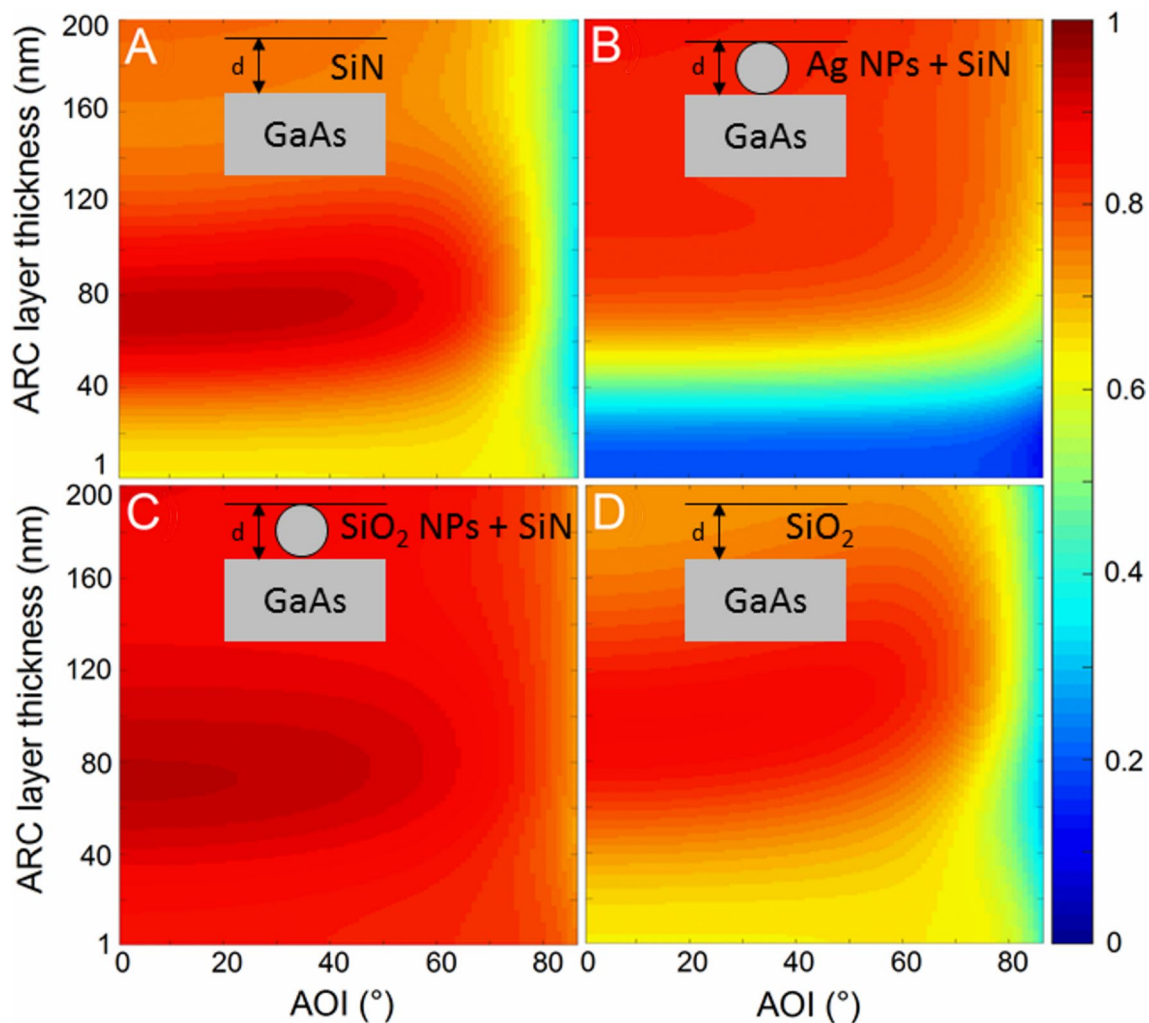


Figure 2. Weighted solar power transmittance (T_w) from (A) thin film SiN ARC, (B) hybrid ARC (Ag NPs + SiN), (C) hybrid ARC (SiO₂ NPs + SiN), and (D) thin film SiO₂ ARC. d : thickness of the ARC layer. The diameter of NPs is equal to the thickness of ARC layer. The contours of hybrid ARC (NPs + SiN) are for 70% surface filling density. 0° AOI corresponds to normal incidence.

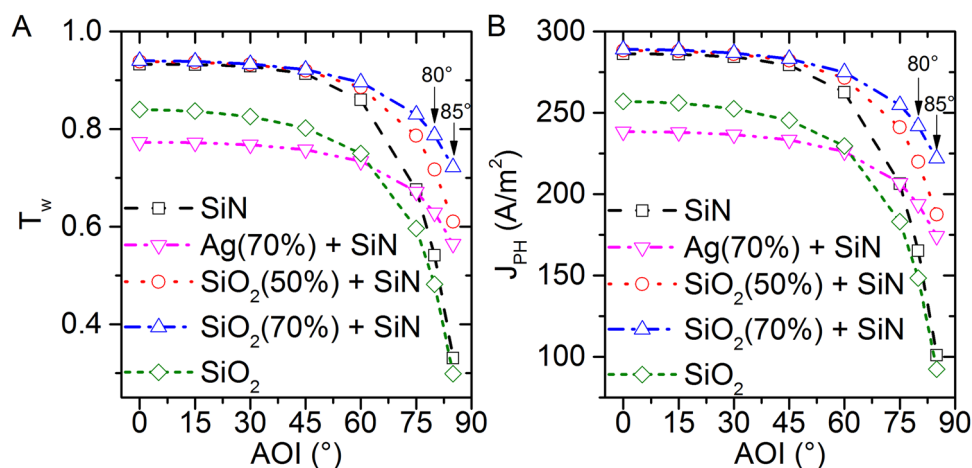


Figure 3. (A) Weighted solar power transmittance (T_w), and (B) photocurrent density (J_{ph}) for 70 nm thick ARC layer. The diameter of NPs are equals to the thickness of ARC layer. Ag (70%) + SiN : the surface filling density of Ag NPs is 70% in the hybrid ARC.

ARC type	Munich, Germany (Lat. = 48.13°)		Chennai, India (Lat. = 13.07°)		Perth, Australia (Lat. = - 31.93°)		Antofagasta, Chile (Lat. = - 23.43°)	
	Opt. = 33°	45°	Opt. = 13°	45°	Opt. = 27°	45°	Opt. = 22°	45°
SiN ARC	0.85	0.85	0.87	0.82	0.87	0.85	0.87	0.84
Hybrid ARC	0.89	0.88	0.93	0.88	0.92	0.89	0.92	0.89
% Increase	4.71	3.53	6.89	7.32	5.75	4.71	5.75	5.95

Table 1. Normalized photocurrent density over the course of a year (2020) at different locations (Lat.: latitude; Opt.: optimum tilt angle; Hybrid ARC: SiO₂ (70%) + SiN).

photocurrent density over the course of a year w. r. t. the normal incidence by using the following expressions at different locations which is summarized in Table 1.

$$J_{PH(inoneday)} = \frac{1}{dayduration(inminutes)} \int_{sunrise}^{sunset} norm.J_{PH}dt(inminutes) \quad (1)$$

To calculate over the course of a year, average J_{PH} is calculated for each of the day of a year using Eq. 1 and summed over. The summation is divided by total no. of days in a year. AOI of the sunlight at the GaAs layer changes at every minute of the day and was calculated by the formula given in Ref.²⁸. The GaAs layer is assumed to face due south in the Northern Hemisphere, or due north in the Southern Hemisphere. We compared the normalized photocurrent density at two different tilt angles cases for the given location: optimum tilt angle²⁹ and 45°. The sun position calculation was done with a freely available MATLAB code³⁰. The improvement in hybrid ARC is clearly noticed at every location. The change due to hybrid ARC is more when the tilt angle is far from the optimum tilt angle (Table 1). Overall, the hybrid ARC has shown improvement in the antireflection property and recommended to use in solar cells.

To the best of our knowledge, the simulated device structure in this study has not been yet reported theoretically or experimentally. Other structures such as NPs layer on a solar cell absorber^{1,8,10-12,14,19}, NPs layer on a thin film ARC layer with an absorber layer^{13,16,19} or NPs fully buried inside a thin film ARC layer with an absorber layer³¹ have been studied extensively. Ha et al. have reported more than 8% enhancement in the current density with 70% surface coverage by SiO₂ NPs on a GaAs solar cell at normal incidence comparing to a bare GaAs solar cell¹¹. The enhancement is also noticed at non-normal AOI. However, the sunlight still faces high reflection in the vicinity of NPs due to the host medium (air) at normal and non-normal AOI. In our device structure, the vicinity is filled with dielectric SiN host medium. At normal incidence, both the thin film SiN ARC and SiO₂ NPs show approximately equal T_W (a small insignificant increase at 0° AOI is noticeable in Fig. 3). But, due to constructive interference at the front surface, the thin film SiN ARC show decrease in T_W at higher AOI whereas NPs don't show this behavior, as reported in Ref. 23²³. As a result, enhancement in T_W at higher AOI has been noticed for hybrid ARC (SiO₂ NPs + SiN) case (Figs. 2C, 3). Starowicz et al. have grown an ARC structure similar to ours in which metal NPs are successfully embedded in a TiOx thin film layer³². The ARC shows 5% increase in the short circuit current at normal incidence. In this case, the TiOx film is deposited with sol-gel method. Similarly, SiN thin film can also be deposited as reported in Ref.³³, nevertheless no results of SiN deposition on a solar cell device structure have been reported by using this method due to complexity in synthesis and non-uniformity in the SiN structure. The controlled size homogeneity and distribution of NPs are also a difficult task, but it can be approximated on a device surface by density distribution calculation^{31,34}. Lesina et al. modelled and characterize Ag NPs embedded in a SiO₂ ARC³¹. In this case, Ag NPs are fully buried inside the thin ARC layer. Furthermore, NP's size and surface coverage have been obtained with the density distribution calculation using ImageJ software. From the fabrication point of view, metal NPs can be synthesized by evaporation of its metal thin films, followed by thermal annealing³⁴⁻³⁶. However, NPs are also commercially available with various manufacturer such as nanoComposix, Inc.¹⁰. Hence, our simulated device structure can be studied experimentally in future and can also be used to guide future experimental design for wide angle antireflection coating and to predict its performance.

In summary, we performed an analytical study which suggests that a combination of $\lambda/4$ coating ARC with dielectric SiO₂ NPs (hybrid ARC) improves the photocurrent density in a GaAs layer at higher AOI. We obtained more than 100% enhancement in the photocurrent density at 85° AOI. Sunrise to sunset calculation of the normalized photocurrent density have also shown improvement in the hybrid ARC case. In future, solar cells integrated into buildings, cars, etc. might become more important. In these cases, the panels are typically not oriented toward the sun and they have to deal with AOI far from the normal incidence. Conventional $\lambda/4$ coating ARC such as thin film SiN ARC is generally optimized for a certain AOI (typically close to normal incidence). Therefore, the hybrid ARC gives a route to alleviate the unwanted reflection at higher AOI and increase the overall efficiency of a solar cell.

Methods

The simulation study is performed using an analytical model²³ which is a combination of Transfer matrix method (TMM), Dipole model and Mie theory. A self-generated MATLAB code is used to solve Mie theory for the scattering efficiency of metal and dielectric NPs. Using the dipole model, an angular distribution of dipole radiation

by a NP in the neighboring substrate is obtained which is later used to calculate the total diffuse scattering (reflected and transmitted) by a NP. The total transmittance is calculated with a linear summation of specular transmittance and diffuse transmittance in which the specular transmittance is calculated with the TMM method and the diffuse transmittance is calculated by the diffuse scattering of NPs.

Assuming a perfect absorber layer (IQE = 1) based solar cell device, the transmittance obtained from the analytical model is used to calculate the photogenerated current density. For the angle of incidence (AOI) of the sunlight on a solar cell surface, the sun's position is calculated by a freely available MATLAB code³⁰.

Received: 11 May 2020; Accepted: 25 September 2020

Published online: 13 October 2020

References

- Schaadt, D. M., Feng, B. & Yu, E. T. Enhanced semiconductor optical absorption via surface plasmon excitation in metal nanoparticles. *Appl. Phys. Lett.* **86**, 063106 (2005).
- Hong, L. *et al.* Design principles for plasmonic thin film GaAs solar cells with high absorption enhancement. *J. Appl. Phys.* **112**, 054326 (2012).
- Derkacs, D., Lim, S. H., Matheu, P., Mar, W. & Yu, E. T. Improved performance of amorphous silicon solar cells via scattering from surface plasmon polaritons in nearby metallic nanoparticles. *Appl. Phys. Lett.* **89**, 093103 (2006).
- Ouyang, Z. *et al.* Nanoparticle: enhanced light trapping in thin-film silicon solar cells. *Prog. Photovolt. Res. Appl.* **19**, 917–926 (2011).
- Nakayama, K., Tanabe, K. & Atwater, H. A. Plasmonic nanoparticle enhanced light absorption in GaAs solar cells. *Appl. Phys. Lett.* **93**, 121904 (2008).
- Li, X. H., Li, P. C., Hu, D. Z., Schaadt, D. M. & Yu, E. T. Light trapping in thin-film solar cells via scattering by nanostructured antireflection coatings. *J. Appl. Phys.* **114**, 044310 (2013).
- Kerker, M., Wang, D. S. & Giles, C. L. Electromagnetic scattering by magnetic spheres. *J. Opt. Soc. Am.* **73**, 765–767 (1983).
- Baryshnikova, K. V., Petrov, M. I., Babicheva, V. E. & Belov, P. A. Plasmonic and silicon spherical nanoparticle antireflective coatings. *Sci. Rep.* **6**, 22136 (2016).
- Akimov, Y. A., Koh, W. S., Sian, S. Y. & Ren, S. Nanoparticle-enhanced thin film solar cells: metallic or dielectric nanoparticles?. *Appl. Phys. Lett.* **96**, 073111 (2010).
- Matheu, P., Lim, S. H., Derkacs, D., McPheeters, C. & Yu, E. T. Metal and dielectric nanoparticle scattering for improved optical absorption in photovoltaic devices. *Appl. Phys. Lett.* **93**, 113108 (2008).
- Ha, D., Yoon, Y. & Zhitenev, N. B. Nanoscale imaging of photocurrent enhancement by resonator array photovoltaic coatings. *Nanotechnology* **29**, 145401 (2018).
- Ha, D., Gong, C., Leite, M. S. & Munday, J. N. Demonstration of resonance coupling in scalable dielectric microresonator coatings for photovoltaics. *ACS Appl. Mater. Interfaces* **8**, 24536–24542 (2016).
- Wan, D. *et al.* Antireflective nanoparticle arrays enhance the efficiency of silicon solar cells. *Adv. Funct. Mater.* **20**, 3064–3075 (2010).
- Ha, D. & Zhitenev, N. B. Improving dielectric nanoresonator array coatings for solar cells. *Part. Part. Syst. Charact.* **35**, 1800131 (2018).
- Tong, Y. *et al.* Photonic enhanced thin-film solar cells with conformal nanostructure. *Sol. Energy* **173**, 504–510 (2018).
- Nagel, J. R. & Scarpulla, M. A. Enhanced absorption in optically thin solar cells by scattering from embedded dielectric nanoparticles. *Opt. Express* **18**, A139–A146 (2010).
- Yeh, Y.-M., Wang, Y.-S. & Li, J.-H. Enhancement of the optical transmission by mixing the metallic and dielectric nanoparticles atop the silicon substrate. *Opt. Express* **19**, A80 (2011).
- Ismail Abdelrahman, M., Rockstuhl, C. & Fernandez-Corbaton, I. Broadband suppression of backscattering at optical frequencies using low permittivity dielectric spheres. *Sci. Rep.* **7**, 14762 (2017).
- Zhao, Y., Chen, F., Shen, Q. & Zhang, L. Optimal structure of light trapping in thin-film solar cells: dielectric nanoparticles or multilayer antireflection coatings?. *Appl. Opt.* **53**, 5222 (2014).
- Huang, W. H. *et al.* UV-visible light-trapping structure of loosely packed submicrometer silica sphere for amorphous silicon solar cells. *IEEE Electron Device Lett.* **33**, 1036–1038 (2012).
- Mertz, J. Radiative absorption, fluorescence, and scattering of a classical dipole near a lossless interface: a unified description. *J. Opt. Soc. Am. B* **17**, 1906–1913 (2000).
- Abelès, F. (1950) La théorie générale des couches minces. *LE J. Phys. LE Radium* **11**, 307–309 (1950).
- Singh, B., Shabat, M. M. & Schaadt, D. M. Wide angle antireflection in metal nanoparticles embedded in a dielectric matrix for plasmonic solar cells. *Prog. Photovolt. Res. Appl.* **28**, 682–690 (2020).
- Palik, E. D. *Handbook of Optical Constants of Solids* (Academic Press, New York, 1998).
- Bouhafs, D., Moussi, A., Chikouche, A. & Ruiz, J. M. Design and simulation of antireflection coating for optoelectronic devices: application to silicon solar cells. *Sol. Energy Mater. Sol. Cells* **52**, 79–93 (1998).
- Bohren, C. F. How can a particle absorb more than the light incident on it? *Am. J. Phys.* **51**, 323 (1983).
- Boden, S. A. & Bagnall, D. M. Sunrise to sunset optimization of thin film antireflective coatings for encapsulated, planar silicon solar cells. *Prog. Photovolt. Res. Appl.* **17**, 241–252 (2009).
- Kalogirou, S. A. *Solar Energy Engineering: Processes and Systems*. Elsevier Inc. (Elsevier Inc., Amsterdam, 2009). <https://doi.org/10.1016/b978-0-12-374501-9.00014-5>
- Jacobson, M. Z. & Jadhav, V. World estimates of PV optimal tilt angles and ratios of sunlight incident upon tilted and tracked PV panels relative to horizontal panels. *Sol. Energy* **169**, 55–66 (2018).
- Droste, R. MATLAB Central File Exchange, sunRiseSet (lat, lng, UTCoff, date, PLOT) (<https://www.mathworks.com/matlabcentral/fileexchange/62180-sunriset-lat-lng-utcoff-date-plot>). Retrieved April 18, 2020 (2020).
- Lesina, A. C. *et al.* Modeling and characterization of antireflection coatings with embedded silver nanoparticles for silicon solar cells. *Plasmonics* **10**, 1525–1536 (2015).
- Starowicz, Z. *et al.* Antireflection TiO_x coating with plasmonic metal nanoparticles for silicon solar cells. *Plasmonics* **8**, 41–43 (2013).
- Shinde, N., Takano, Y., Sagan, J., Monreal, V. & Nagahara, T. Spin-on silicon-nitride films for photo-lithography by RT cure of polysilazane. *J. Photopolym. Sci. Technol.* **23**, 225–230 (2010).
- Temple, T. L., Mahanama, G. D. K., Reehal, H. S. & Bagnall, D. M. Influence of localized surface plasmon excitation in silver nanoparticles on the performance of silicon solar cells. *Sol. Energy Mater. Sol. Cells* **93**, 1978–1985 (2009).
- Schmid, M., Klenk, R., Lux-steiner, M. C., Topič, M. & Krč, J. Modeling plasmonic scattering combined with thin-film optics. *Nanotechnology* **22**, 025204 (2011).

36. Morawiec, S. *et al.* Self-assembled silver nanoparticles for plasmon-enhanced solar cell back reflectors: correlation between structural and optical properties. *Nanotechnology* **24**, 265601 (2013).

Author contributions

D.M.S. proposed the idea and guided the study. B.S. performed the MATLAB simulations and result analysis. B.S. wrote the main manuscript. M.M.S. was involved in the discussion. All the authors reviewed the manuscript.

Funding

Open Access funding enabled and organized by Projekt DEAL.

Competing interests

The authors declare no competing interests. Additional information

Correspondence and requests for materials should be addressed to B.S.

Reprints and permissions information is available at www.nature.com/reprints.

Publisher's note Springer Nature remains neutral with regard to jurisdictional claims in published maps and institutional affiliations.



Open Access This article is licensed under a Creative Commons Attribution 4.0 International License, which permits use, sharing, adaptation, distribution and reproduction in any medium or format, as long as you give appropriate credit to the original author(s) and the source, provide a link to the Creative Commons licence, and indicate if changes were made. The images or other third party material in this article are included in the article's Creative Commons licence, unless indicated otherwise in a credit line to the material. If material is not included in the article's Creative Commons licence and your intended use is not permitted by statutory regulation or exceeds the permitted use, you will need to obtain permission directly from the copyright holder. To view a copy of this licence, visit <http://creativecommons.org/licenses/by/4.0/>.

© The Author(s) 2020